A Novel Time-Domain Algorithm for Synthesizing Broadband Macromodels of Coupled Interconnects

Tzong-Lin Wu, *Member, IEEE*, Chun-Chih Kuo, Chen-Chao Wang, Sung-Moa Wu, and Chih-Pin Hung

***Abstract*—Based on a novel multidimensional deconvolution algorithm (MDA), this paper proposes a time-domain approach to synthesize the broadband SPICE-compatible macromodels of coupled interconnects. The multiple conductor interconnects are excited either experimentally by TDR or numerically by the step-like source in finite difference time domain (FDTD) method. According to the time-domain scattered data, the macromodel of the interconnect can be efficiently extracted by cascading several configuration-oriented coupled transmission lines (CCTL). Two examples are used to demonstrate the validity of the proposed approach. One is the equivalent models for differential pairs crossing an asymmetrical ground slot. The other is the crosstalk behavior prediction for a three-coupled microstrip line. The accuracy in broadband frequency range of the synthesized models of these two examples are checked both in time and frequency domain and compared with the direct-FDTD simulation. The agreement is favorably good.**

***Index Terms*—Crosstalk, differential interconnects, FDTD, macromodels, signal integrity, SPICE-compatible model, TDR.**

I. Introduction

With rapidly increasing clock rate and interconnect layout density in the digital or mixed circuits, the coupled noise (or crosstalk) between neighboring interconnects can be a critical factor to degrade the signal integrity (SI) in package design. In order to accurately perform overall system-level SI simulation, extracting the SPICE-compatible models with the crosstalk effect being considered in the multiconductor interconnects and incorporating the model into the conventional circuit simulator, such as SPICE, is essential.

The SPICE-compatible models of the coupled interconnects can be constructed from either frequency-domain or time-domain data [1], [2]. According to the simulated or measured scattering (S)-parameters, several systematic approaches have been proposed to extract the macromodels of the coupled interconnects [3]–[10]. The multiport S-parameter or impedance matrix is first represented by a rational functions matrix. The stability and passivity of the extracted circuits are enforced through constraints on the poles and residuals of the rational functions. Equivalent lumped circuits are then generated from the modified rational functions. Those approaches can obtain accurate and broadband models. However, time-domain measurement, like TDR/TDT, or time-domain numerical simulation, like finite difference time domanin (FDTD) method [11], [12], is becoming popular and important for high-speed digital circuits design. It will be more convenient to construct the SPICE-compatible models directly employing the time-domain scattered data. Several works based on the layer peeling technique have been contributed to the equivalent model extraction from the time-domain data [13]–[15], but they focus on a single interconnect. To extract the crosstalk parameters of the multiport interconnects such as differential interconnect in time-domain, multiple step sources are needed to simultaneously excite the coupled interconnects and the integration formulations in time-domain are then used to calculate the mutual coupling parameters [16]–[19]. The problem of this approach is that as the number of the coupled interconnects is increased, many excitations are needed and the cost is increased in measurement. Another issue is that the formulation of the crosstalk parameters becomes complicated for increasing the port numbers.

In this paper, based on a novel multidimensional deconvolution algorithm (MDA), a time-domain approach is proposed to synthesize the SPICE-compatible macromodels of the coupled interconnects. In this approach, only one excitation source is needed. According to the scattered voltage waveform in time-domain at each port with changing the excitation port respectively, the macromodel using cascaded coupled transmission line systems can be efficiently synthesized by the novel MDA. The stability and passivity are kept for the macromodel because each synthesized unit is in passive causal mode. The proposed approach can be applied to the time-domain data either from TDR measurement or FDTD simulation.

The algorithm of MDA is derived at Section II. Two examples are used to demonstrate the validity of the proposed approach in Section III. They are differential pairs crossing asymmetrical slotted ground and a three coupled interconnects on PCB. Both the frequency- and time-domain response of the extracted macromdels are compared with the results directly calculated by FDTD method. Final section is the conclusions.

II. Multidimensional Deconvolution Algorithm (MDA)

A. Scattered Voltage Waveforms in Time-Domain

Consider a nonuniform $N+1$-conductor coupled interconnects as shown in Fig. 1, where conductor 0 is the reference ground and conductors from 1 to N are the signal traces. To understand the crosstalk behavior between any two conductors, the time domain scattered voltages, which is denoted as $V_{mn}(t)$, have to be recorded at the near-end of conductor m (or port m) with the step source $S(t)$ being excited at the near-end of conductor n (or port n), where $n = 1, 2, \ldots N$, and $m =$

Manuscript received August 15, 2003; revised January 14, 2004. This work was supported in part by the National Science Council, Taiwan, R.O.C. under Grant 92-2213-E-110-013 and the Ministry of Education, Program for Promoting Academic Excellence of Universities under Grant A-91-EFA08-1-4.

T.-L. Wu, C.-C. Kuo, and C.-C. Wang are with the Department of Electrical of Engineering, National Sun Yat-sen University, Kaohsiung 80424, Taiwan, R.O.C. (e-mail: wtl@mail.ee.nsysu.edu.tw).

S.-M. Wu and C.-P. Hung are with the Core Capability Center, Advanced Semiconductor Engineering, Inc., Taipei, Taiwan, R.O.C.

Digital Object Identifier 10.1109/TADVP.2004.825456

1521-3323/04$20.00 © 2004 IEEE

Authorized licensed use limited to: Sungmao Wu. Downloaded on May 24,2021 at 05:59:05 UTC from IEEE Xplore. Restrictions apply.

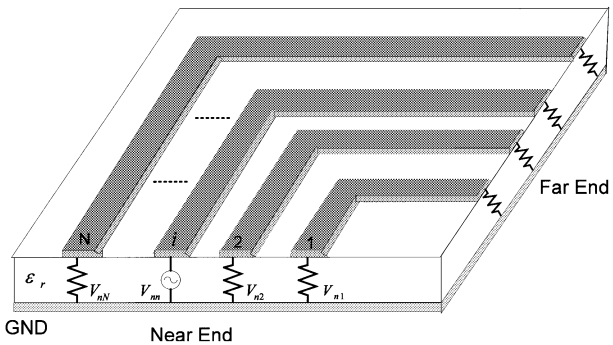

Fig. 1. Schematic of the nonuniform N + 1 multiconductor coupled interconnects.

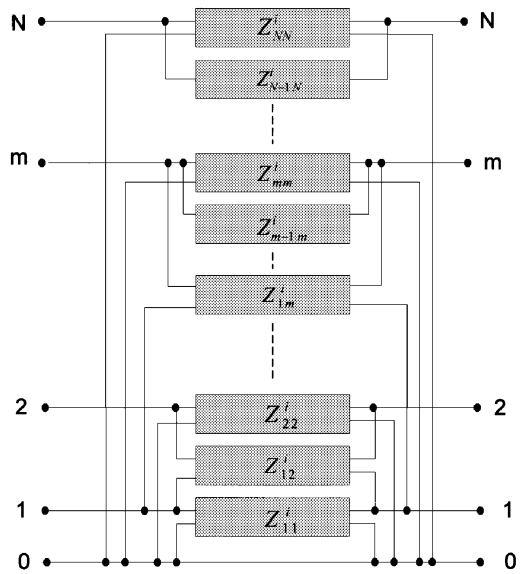

Fig. 2. One segment of the cascade of piecewise uniform N + 1 coupled line units.

$1, 2, \ldots N$. For convenience of following macromodel extraction, all the near and far ends of the multiconductor transmission system are terminated with 50Ω loads.

B. Formulations of the MDA

To fit the time-domain response of the $N+1$-conductor coupled interconnects, we use the configuration-oriented coupled transmission lines (CCTL) as a unit basis (or a section) to construct the macromodel of general coupled interconnects. By cascading several CCTL section with different propagation characteristics, arbitrary time-domain response waveform can be synthesized. The reason we call macromodel is that each CCTL unit is not necessary to correlate with physical structure of the coupled interconnects at each corresponding cross-section. Fig. 2 shows a CCTL unit for the $N+1$-conductor coupled interconnects. It consists of M ideal transmission lines of the same length Δx and propagation delay $\Delta t = \Delta x/v$, where $M = N(N+1)/2$ and v is the propagation velocity of the CCTL section. The characteristic impedance of the M transmission lines at section i is denoted as Z^i_{nm} ($n = 1, 2, \ldots, N$ and $m = n, n+1, \ldots, N$) which represents the impedance between conductor n and m if $n \neq m$ and the impedance between conductor n and the conductor 0 (reference ground) if $n = m$.

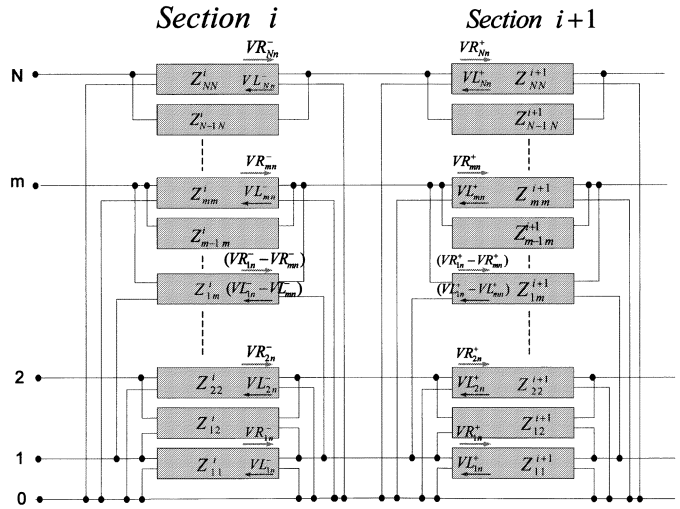

Fig. 3. Relative right- and left-traveling voltage waves at the junction between the Z^{i-1}_{nm} and Z^i_{nm} transmission lines.

The MDA is used to synthesize the corresponding propagation characteristics of each CCTL according to the scattered voltage waveform $V_{mn}(t)$ with $n, m = 1, 2, \ldots N$. We first decompose the time-domain voltage waveform at the conductor m to the right-traveling $VR_{mn}(x,t)$ and left-traveling $VL_{mn}(x,t)$ voltage wave, where the step source is excited at conductor n and x is the position of the transmission system. As shown in Fig. 3, the right- and left-traveling voltage wave at the junction between the Z^{i-1}_{nm} and Z^i_{nm} transmission lines, where $m = 1, 2, \ldots, N$, can be discretized as

$$VL^-_{mn}(i,j) = VL(x = i\Delta x - \varepsilon, t = (i + 2(j-1))\Delta t) \tag{1a}$$

$$VL^+_{mn}(i,j) = VL(x = i\Delta x + \varepsilon, t = (i + 2(j-1))\Delta t) \tag{1b}$$

$$VR^-_{mn}(i,j) = VR(x = i\Delta x - \varepsilon, t = (i + 2(j-1))\Delta t) \tag{1c}$$

$$VR^+_{mn}(i,j) = VR(x = i\Delta x + \varepsilon, t = (i + 2(j-1))\Delta t) \tag{1d}$$

where $\varepsilon \to 0$ and the source is excited at port n with $n = 1, 2, \ldots, N$.

From the continuity of voltage and current at conductor m (or port m) between sections $i-1$ and i, we have (2a) and (2b) shown at the bottom of the next page.

Applying (2a) and (2b) from port 1 to port N, i.e., $m = 1, 2, \ldots, N$, a transfer matrix form of voltage variables $\overline{VR^+_n}(i,j)$ and $\overline{VL^+_n}(i,j)$ can be expressed as

$$\begin{bmatrix} \overline{VR^+_n}(i,j) \\ \overline{VL^+_n}(i,j) \end{bmatrix}_{2N\times 1} = \begin{bmatrix} \bar{I} & \bar{I} \\ \bar{Z}_i & -\bar{Z}_i \end{bmatrix}^{-1}_{2N\times 2N} \times \begin{bmatrix} \bar{I} & \bar{I} \\ \bar{Z}_{i-1} & -\bar{Z}_{i-1} \end{bmatrix}_{2N\times 2N} \begin{bmatrix} \overline{VR^-_n}(i,j) \\ \overline{VL^-_n}(i,j) \end{bmatrix}_{2N\times 1} \tag{3}$$

where $\bar{I}$ is the unit vector of degree N, the column vector $\overline{VR^+_n}(i,j) = [VR^+_{1n}(i,j), VR^+_{2n}(i,j), \ldots, VR^+_{Nn}(i,j)]^T$, the column vector $\overline{VL^+_n}(i,j) = [VL^+_{1n}(i,j), VL^+_{2n}(i,j), \ldots,$

Authorized licensed use limited to: Sungmao Wu. Downloaded on May 24,2021 at 05:59:05 UTC from IEEE Xplore. Restrictions apply.

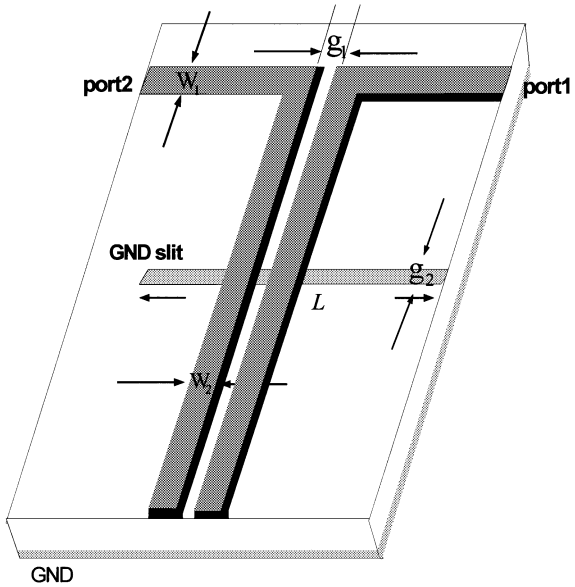

Fig. 4. Modeling structure of the differential pairs crossing asymmetrical ground slot with $W_1 = W_2 = 0.729$ mm, $g_1 = 0.365$ mm, $g_2 = 0.1216$ mm, $L = 16.4$ mm in FR4 board with the dimension of 2.07 cm × 2.59 cm × 0.4 mm.

$\mathrm{VL}^{+}_{Nn}(i,j)]^T, \overline{VR^{-}_{n}}(i,j)$ and $\overline{VL^{-}_{n}}(i,j)$ are similarly defined, and (4), shown at the bottom of the page, with reciprocity of $Z^i_{km} = Z^i_{mk}$.

A key point of the synthesis concept is that the multiconductor coupled transmission lines have been broken into sections of electrical length Δt, while the excitation and response functions are discretized into sections of length $2\Delta t$. Because a change in the reflected waves caused by junction $i+1$ occurs no sooner than $2\Delta t$ after that due to junction i, the impedance matrix $\bar{Z}_i$ can be obtained by the first time interval data ($j = 1$) of right-traveling and left-traveling waves, i.e., $\overline{VR^{-}_{n}}(i,1)$ and $\overline{VL^{-}_{n}}(i,1)$, at junction i with $\overline{VL^{+}_{n}}(i,1) = 0$

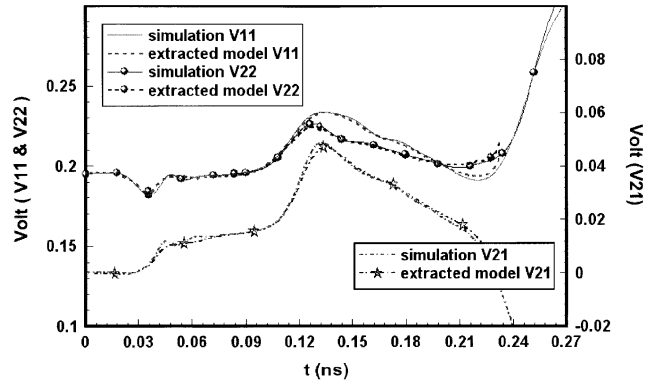

Fig. 5. Comparison of time-domain voltage wave $V_{11}(t), V_{22}(t)$, and $V_{21}(t)$ between extracted model and the simulation by FDTD.

and $\overline{VR^{+}_{n}}(i,1) = \overline{VR^{-}_{n}}(i,1) + \overline{VL^{-}_{n}}(i,1)$. Therefore, the relation of the impedance matrix between $\overline{Z_i}$ and $\overline{Z_{i-1}}$ can be expressed as

$$\overline{Z_i}(\overline{VR^{-}_{n}}(i,1) + \overline{VL^{-}_{n}}(i,1)) = \overline{Z_{i-1}}(\overline{VR^{-}_{n}}(i,1) - \overline{VL^{-}_{n}}(i,1)) \quad (5)$$

by rearranging (4). Changing the excitation port n from 1 to N, the impedance matrix at section i is synthesized as

$$\overline{Z_i} = \overline{Z_{i-1}}\bar{P}\bar{Q}^{-1} \quad (6)$$

where $\bar{P} = (\overline{p_1}, \overline{p_2}, \ldots, \overline{p_N})$ with column vector $\overline{p_n} = \overline{VR^{-}_{n}}(i,1) - \overline{VL^{-}_{n}}(i,1)$ and $\bar{Q} = (\overline{q_1}, \overline{q_2}, \cdots, \overline{q_N})$ with column vector $\overline{q_n} = \overline{VR^{-}_{n}}(i,1) + \overline{VL^{-}_{n}}(i,1)$.

At this point, (6) has presented how to synthesize the impedance matrix $\bar{Z}_i$ of section i by the first interval time-domain incident wave (or right-traveling) and reflected wave (or left-traveling wave) with varying excitation port from 1 to N. We have also derived the equations such that, given the right- and left-traveling waves to the left of any junction i, we can

$$VL^{-}_{mn}(i,j) + VR^{-}_{mn}(i,j) = VL^{+}_{mn}(i,j) + VR^{+}_{mn}(i,j)\,(VR^{-}_{mn}(i,j) - VL^{-}_{mn}(i,j))/\,Z^i_{mm} \quad (2a)$$

$$+ \sum_{\substack{k=1\\k\neq m}}^{N} (VR^{-}_{mn}(i,j) - VR^{-}_{kn}(i,j))/\,Z^i_{km} - \sum_{\substack{k=1\\k\neq m}}^{N} (VL^{-}_{mn}(i,j) - VL^{-}_{kn}(i,j))/\,Z^i_{km}$$

$$= (VR^{+}_{mn}(i,j) - VL^{+}_{mn}(i,j))/\,Z^{i+1}_{mm} + \sum_{\substack{k=1\\k\neq m}}^{N} (VR^{+}_{mn}(i,j) - VR^{+}_{kn}(i,j))/\,Z^{i+1}_{km}$$

$$- \sum_{\substack{k=1\\k\neq m}}^{N} (VL^{+}_{mn}(i,j) - VL^{+}_{kn}(i,j))/\,Z^{i+1}_{km}. \quad (2b)$$

$$\bar{Z}_i = \begin{bmatrix} \sum_{k=1}^{N} 1/Z^i_{k1} & -1/Z^i_{21} & -1/Z^i_{31} & \cdots & -1/Z^i_{N1} \\ -1/Z^i_{12} & \sum_{k=1}^{N} 1/Z^i_{k2} & -1/Z^i_{32} & \cdots & -1/Z^i_{N2} \\ \vdots & & \ddots & & \vdots \\ -1/Z^i_{1N} & \cdots & \cdots & \cdots & \sum_{k=1}^{N} 1/Z^i_{kN} \end{bmatrix} \quad (4)$$

Authorized licensed use limited to: Sungmao Wu. Downloaded on May 24,2021 at 05:59:05 UTC from IEEE Xplore. Restrictions apply.

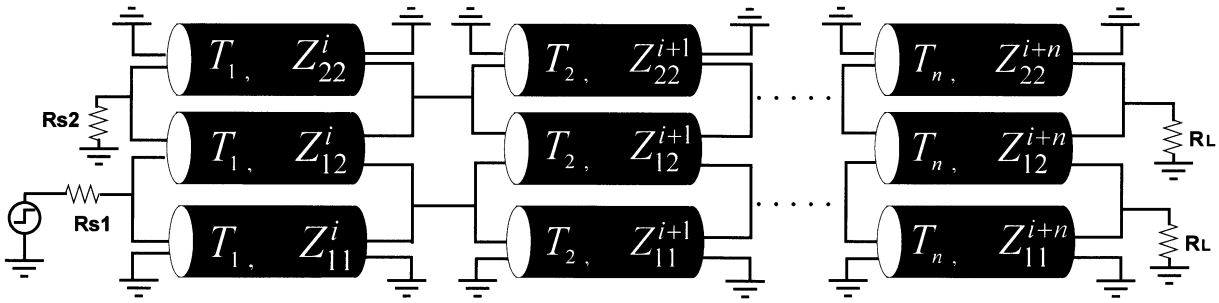

Fig. 6. Equivalent distributed SPICE model of the coupled lines with the asymmetric ground slot.

calculate the right- and left-traveling waves to the right of the junction by (3) if the impedance matrix $\overline{Z_{i-1}}$ and $\overline{Z_i}$ are known. What remains now is to relate the right- and left-traveling waves at junction i to those at junction $i+1$.

Since the translation by Δx along any of the $\overline{Z_i}$ section corresponds to a time shift of $\pm\Delta t$ for the right $(-\Delta t)$ and left $(+\Delta t)$ traveling waves. Using the indexing from (1), we obtain

$$\overline{VR_n^-}(i+1,j) = \overline{VR_n^+}(i,j) \tag{7a}$$

$$\overline{VL_n^-}(i+1,j) = \overline{VL_n^+}(i,j+1) \tag{7b}$$

where $j = 1,2,3,\ldots,L-i$ and L is the sampling numbers of the excitation or response waveform at the near end of the multiconductors system.

This completes the derivations for deconvolution of one layer of the multiconductors transmission lines and a translation to the next junction. The entire process is summarized in the following algorithm.

a) Simulating the time-domain near-end responses of the $N+1$ multiconductors system with locating the excitation source from port 1 to N, respectively. Recording all the voltage waveforms $V_{mn}(t)$ with the exciting port $n = 1,2\ldots N$, and the receiving port $m = 1,2\ldots n$.
b) Based on the notations in (1), the discretized right-traveling and left-traveling waves at the near-ends $(i=1)$ is expressed as

$$\begin{aligned} VR_{nn}^-(1,j) &= S((1+2(j-1))\Delta t) \\ VL_{nn}^-(1,j) &= V_{nn}((1+2(j-1))\Delta t) \\ &\quad - S((1+2(j-1))\Delta t) \end{aligned}$$

and

$$\begin{aligned} VR_{mn}^-(1,j) &= 0 \\ VL_{mn}^-(1,j) &= V_{mn}((1+2(j-1)\Delta t)) \end{aligned}$$

for $m \neq n$, where the time sequence $j = 1,2,\ldots,L$ with sampling period $2\Delta t$.
c) Assume a known $\overline{Z_0}$ and starting with $i=1$.
d) Solve for $\overline{Z_i}$ using (6).
e) Calculate $\overline{VR_n^+}(i,j)$ and $\overline{VL_n^+}(i,j)$ by applying solved $\overline{Z_i}$ at step (d) to (3) for $j = 1,2,\ldots,L+1-i$.
f) Calculate $\overline{VR_n^-}(i+1,j)$ and $\overline{VL_n^-}(i+1,j)$ using (7).
g) Increment i by 1 and repeat steps (d) through (g) until $i = L$.

It is noted that in the proposed MDA the coupled interconnects are synthesized by the lossless CCTL sections. Although the losssy terms are not included in this approach, the accuracy of the macromodels are reasonably good for the practical coupled interconnects with short electrical length.

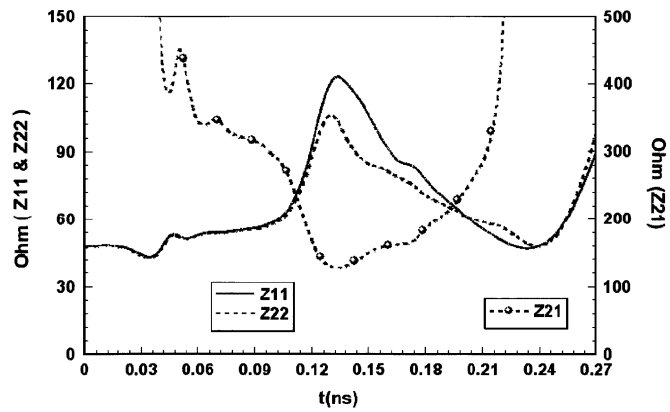

Fig. 7. Synthesized impedance profile of Z_{11}, Z_{22}, and Z_{21} of each CCTL unit along the signal trace.

III. Examples

In this section, two examples are used to demonstrate the applicability of the proposed model extraction approach. One is a differential signal crossing an asymmetrical ground slot. The other example is the crosstalk behavior of signal bus with three traces on a PCB. Fig. 4 shows the schematic of the differential pair on PCB package $(\varepsilon_r = 4.3)$ with an asymmetrical ground slot. The board dimension is 2 cm × 2.6 cm × 0.4 mm and the slot width is 0.12 mm. Each trace of the coupled lines is designed with characteristic impedance 50Ω. The other geometrical parameters are denoted in Fig. 4. The FDTD method is used to simulate the time-domain response of the asymmetrical differential signals, where the corresponding parameters are $\Delta x = \Delta y = 0.12$ mm, $\Delta z = 0.1$ mm, and $\Delta t = 0.18$ ps. A step resistive voltage source of amplitude 0.4 V and rise time 45 ps is excited at port 1 and port 2, respectively. The time-domain scattered data $V_{11}(t), V_{22}(t)$, and $V_{21}(t)$, as shown Fig. 5, is used to synthesize the macromodel of the asymmetrical differential pair. Fig. 6 shows the corresponding CCTL unit consisting ofthree coupled transmission lines $(M=3)$. Fig. 7 shows the synthesized impedance profile of Z_{11}, Z_{22}, and Z_{21} of each CCTL unit along the signal trace. The macromodel of the asymmetrical differential pair can be constructed by cascading 25 CCTL sections. The propagation delay of each CCTL is determined by half of the propagation time of the corresponding section in scattered time-domain voltage waveform. The number of the total

Authorized licensed use limited to: Sungmao Wu. Downloaded on May 24,2021 at 05:59:05 UTC from IEEE Xplore. Restrictions apply.

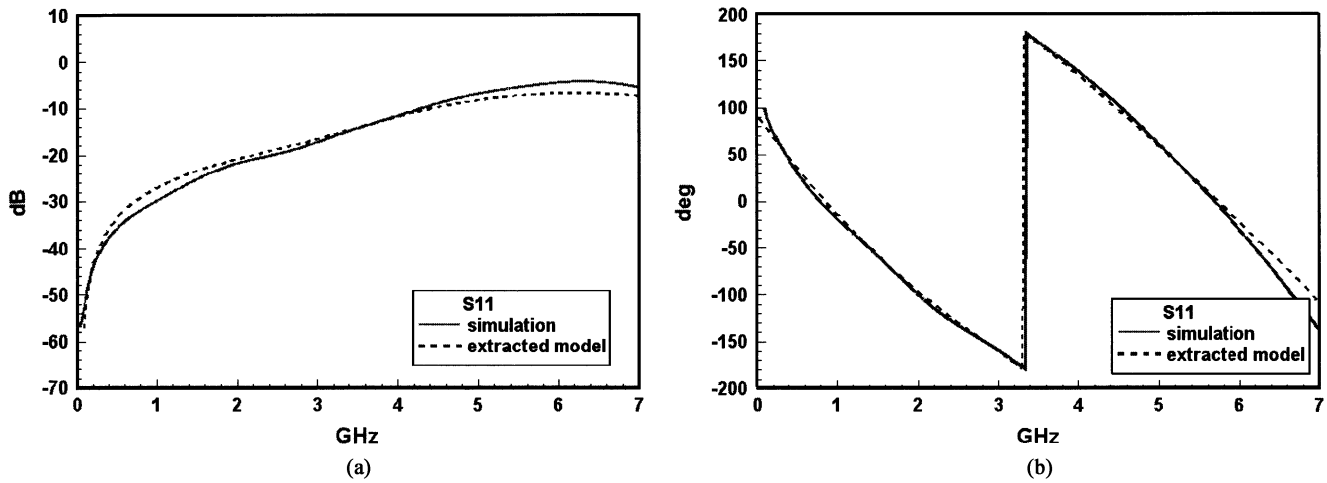

Fig. 8. Comparison of the frequency response S_{11} up to 7 GHz between the FDTD simulation and the extracted model (a) magnitude and (b) phase.

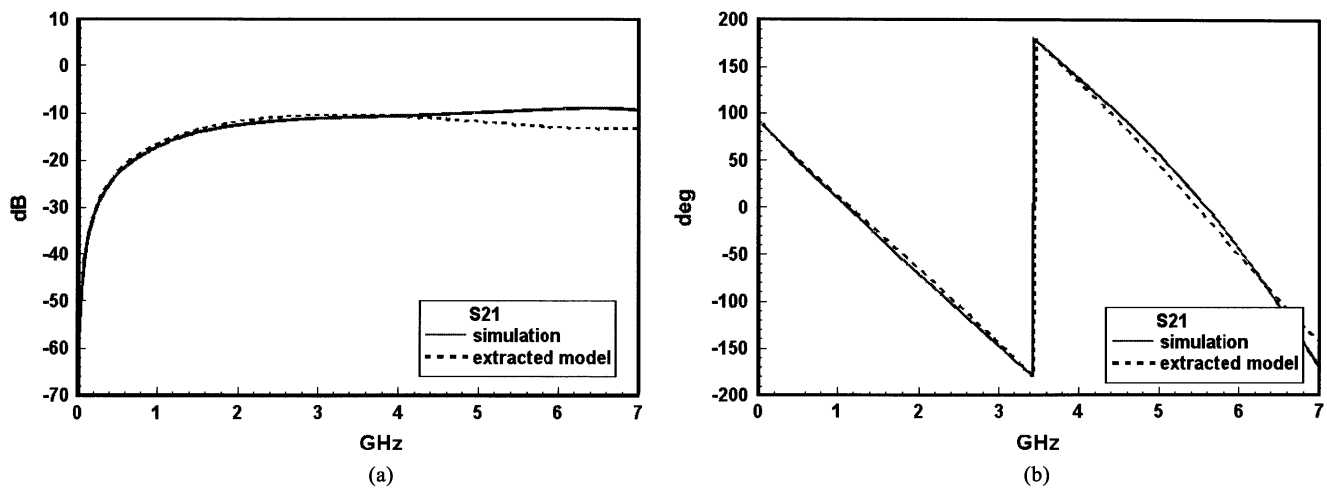

Fig. 9. Comparison of the frequency response S_{21} up to 7 GHz between the FDTD simulation and the extracted model (a) magnitude and (b) phase.

sections is decided by the edge rate of the excitation source and the variation rate of the impedance profile along the coupled traces. The resolution is higher with more sections for larger variation of the impedance distribution along the signal traces. To both keep accuracy and efficiency, it is suggested that for larger impedance variation interconnects the propagation delay of the CCTL section is chosen between 1/20 and 1/5 of the excitation source rise-time.

The accuracy of the synthesized macromodel of the differential pair is checked both in time- and frequency-domain. The time-domain responses ($V_{11}(t), V_{22}(t)$, and $V_{21}(t)$) of the cascaded models are calculated in the SPICE and are also shown in Fig. 5. It is quite consistent with the results simulated by FDTD method. Fig. 8(a) and (b) shows the amplitude and phase of $S_{11}(f)$, respectively. The results calculated both by the macromodel and FDTD method are presented for comparison. The agreement between them is good in broadband frequency from dc to 7 GHz. Fig. 9(a) and (b) show the amplitude and phase of $S_{21}(f)$, respectively. The consistency between the results by the extracted macromodel and FDTD calculation is also good. The reason we show the frequency response only up to 7 GHz is that the rise time of the excitation source is $t_r = 45$ ps, where the bandwidth of the signal source is about $0.35/t_r \cong 7.7$ GHz The higher frequency response can be obtained if the macromodel is synthesized using faster rising edge source.

The schematic of the second example, three parallel traces on a perfect ground plane, is shown in Fig. 10. The characteristic impedance of every single trace is designed as 50Ω. It is a case of four-conductor transmission line with geometrical symmetry to the center trace $(N = 3)$. As shown in Fig. 11, the macromodel of the parallel traces can be synthesized by cascading the CCTL units with $M = 6$. The time-domain scattered data at the near-ends $V_{11}(t) = V_{33}(t), V_{12}(t) = V_{23}(t), V_{22}(t)$, and $V_{13}(t)$ are recorded based on the FDTD simulation with the excitation of resistive step voltage source. The FDTD variables are $\Delta x = \Delta y = 0.251$ mm, $\Delta z = 0.2$ mm, and $\Delta t = 0.3$ ps. Following the model extraction procedures described in Section II, the self-impedance ($Z_{11} = Z_{33}$ and Z_{22}) and mutual-impedance ($Z_{12} = Z_{32}$ and Z_{13}) can be synthesized and are shown in Fig. 12. As shown in Fig. 12, the impedance profiles can be divided into four regions (A to D). Region A is the region where the mutual coupling between any two traces is negligible. Therefore, it is seen that at this region the self-impedance for each trace is kept at 50Ω and the mutual impedance is approaching infinity. Region B is the transition region, where trace 1 and 3 have 90° bend and trace 2 is kept straight. At this region Z_{11}

Authorized licensed use limited to: Sungmao Wu. Downloaded on May 24,2021 at 05:59:05 UTC from IEEE Xplore. Restrictions apply.

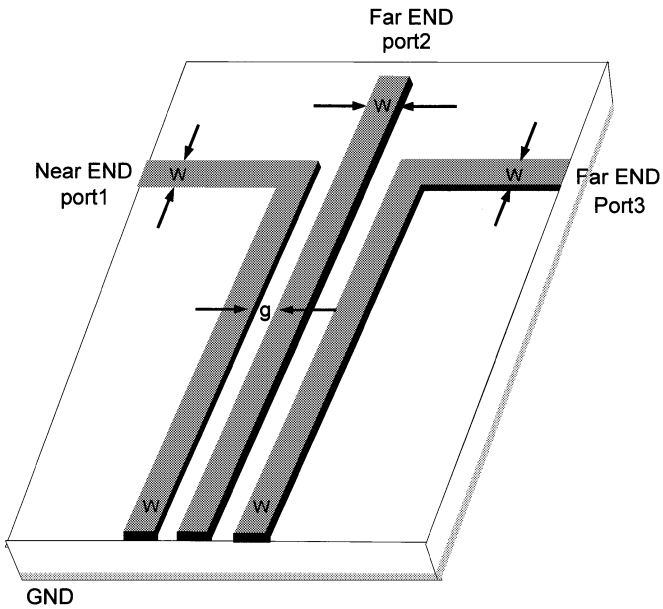

Fig. 10. Modeling structure of the three conductor coupled lines with $W = 1.51$ mm, $g = 0.753$ mm in FR4 board with the dimension of 5.42 cm × 3.81 cm × 0.8 mm.

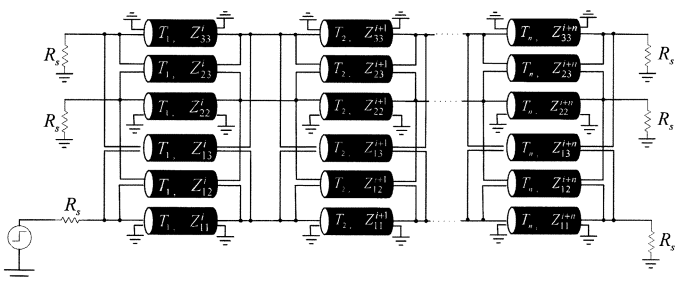

Fig. 11. Equivalent distributed SPICE model of the three conductor coupled lines with a perfect ground plane.

and Z_{33} are changed to about 40Ω due to the bending effect and oscillate to about 60Ω due to the coupling effect of neighboring traces. Z_{22} is directly transited to 70Ω. Region C is the uniform coupling region, where three traces are in parallel. It is seen that Z_{11} and Z_{22} are uniformly kept at about 60Ω and 70Ω, respectively. The last region is the open circuit region, where each trace is terminated with open circuit. It is clearly found that the self-impedances are all approaching infinity.

Based on the synthesized self- and mutual impedances, the equivalent macromodel of the coupled four-conductor interconnects can be established by cascading 24 segments of CCTL units. The comparisons between the time-domain response of the synthesized equivalent model and directly FDTD-simulated behavior are demonstrated in Fig. 13(a) and (b). The time-domain voltage waveforms $V_{11}(t)$ and $V_{21}(t)$ at the near ends are shown in Fig. 13(a), and $V_{22}(t)$ and $V_{13}(t)$ are presented in Fig. 13(b). Agreement between the SPICE-simulated and FDTD-calculated results is favorably good. The accuracy of the extracted models in frequency-domain responses is shown in Figs. 14–16. The amplitude and phase of S_{11} $(=S_{33})$ are shown in Fig. 14(a) and (b), respectively. The corresponding terms of S_{21} $(=S_{23})$ and S_{31} are shown in Figs. 15 and 16,

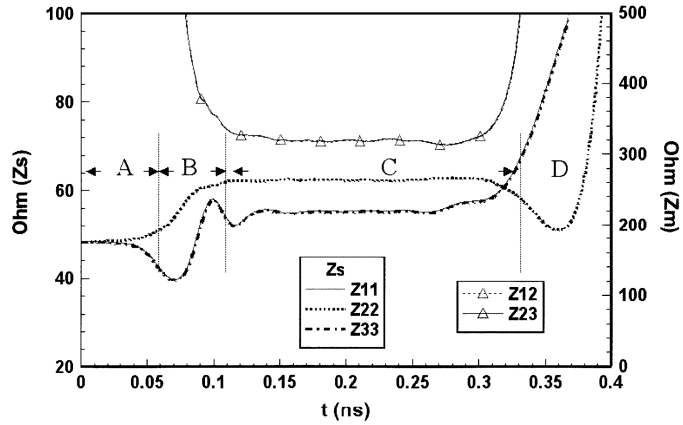

Fig. 12. Impedance profile with mutual- and self-impedance. It can divide into four regions with: (A) noncoupled region, (B) transition region at the 90^{circ} bend, (C) uniform coupled region, and (D) open region.

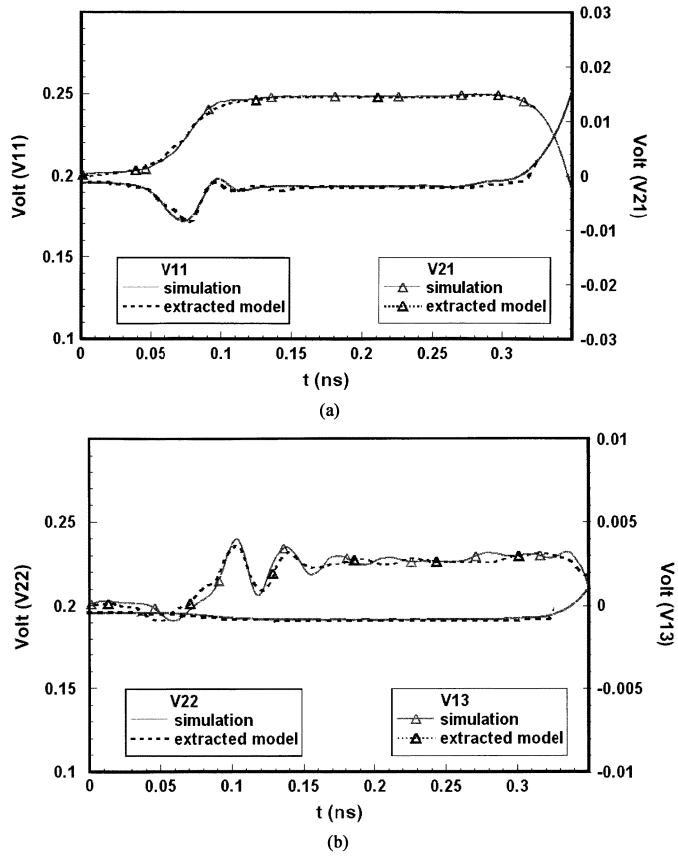

Fig. 13. Comparison of the time-domain response by between the FDTD simulation and the extracted model (a) V_{11} and V_{21} and (b) V_{22} and V_{13}.

respectively. It is seen that the constructed macromodel can well predict the broadband behavior from dc to 7 GHz.

It is emphasized that the proposed MDA can synthesize an appropriate macromodel by cascading several CCTL units based on the time-domain scattered voltage waves. Only one excitation source is needed for extracting the models. The geometrical structures of the coupled interconnects need not to be known in advance. Therefore, this approach is suitable to be applied in the TDR measurement for establishing the models of the coupled interconnects.

Authorized licensed use limited to: Sungmao Wu. Downloaded on May 24,2021 at 05:59:05 UTC from IEEE Xplore. Restrictions apply.

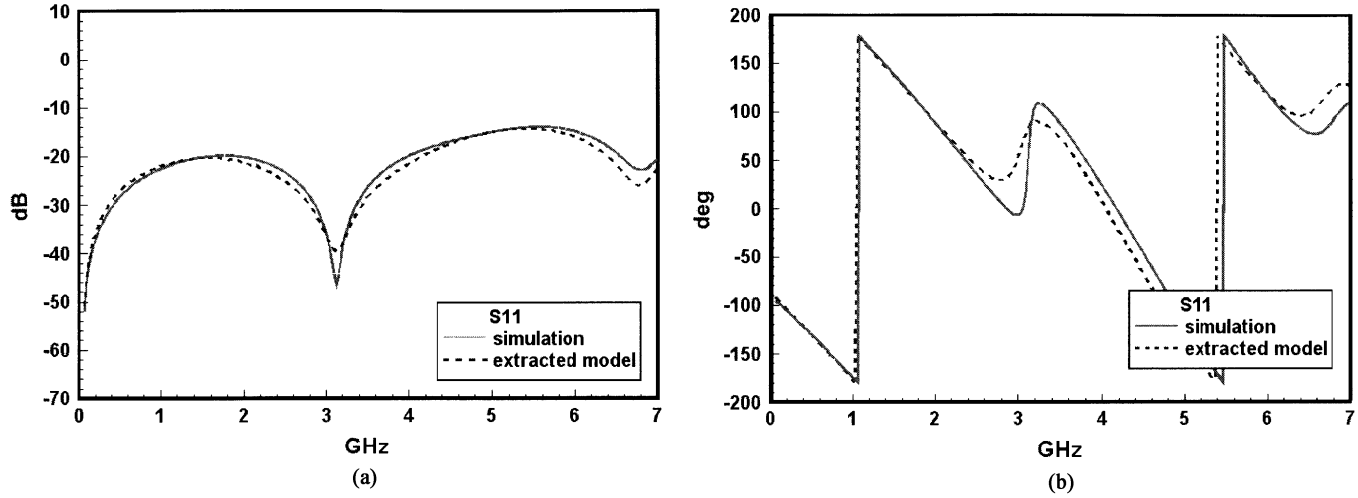

Fig. 14. Comparison of the frequency response S_{11} between the FDTD simulation and the extracted model (a) magnitude and (b) phase.

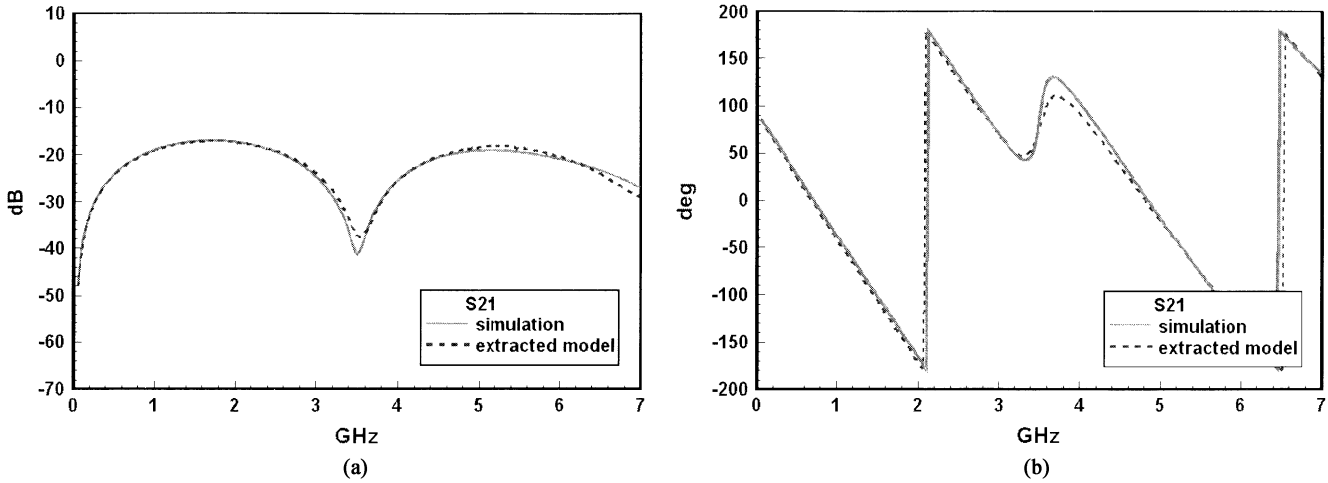

Fig. 15. Comparison of the frequency response S_{21} between the FDTD simulation and the extracted model (a) magnitude and (b) phase.

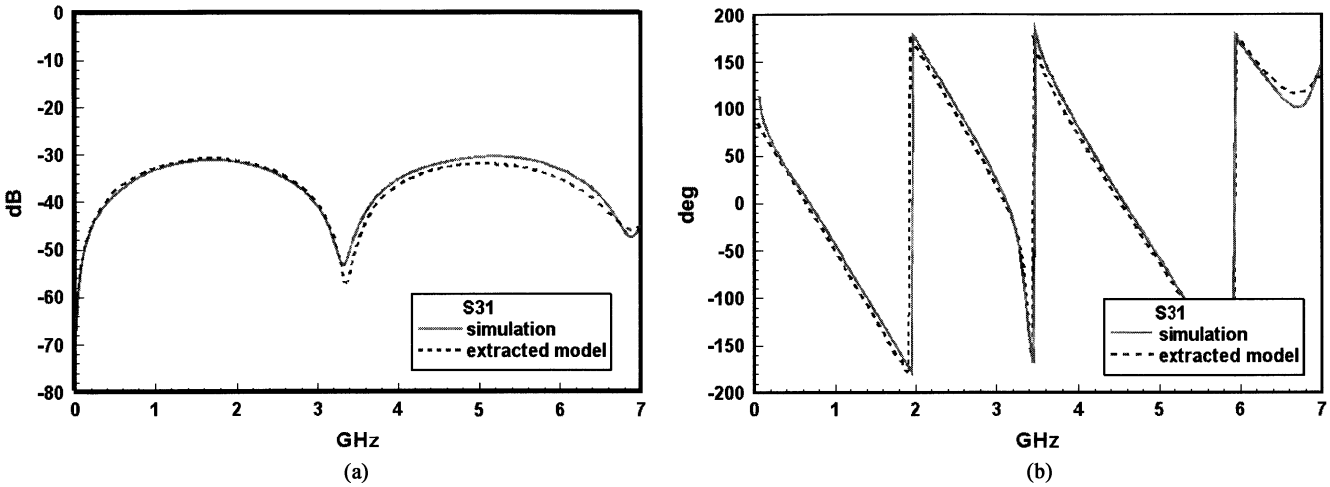

Fig. 16. Comparison of the frequency response S_{31} between the FDTD simulation and the extracted model (a) magnitude and (b) phase.

Authorized licensed use limited to: Sungmao Wu. Downloaded on May 24,2021 at 05:59:05 UTC from IEEE Xplore. Restrictions apply.

IV. Conclusion

Based on the scattered time-domain voltage either measured by TDR or simulated by FDTD, a novel multidimensional deconvolution algorithm (MDA) is proposed to synthesize the broadband macromodel of the multiconductor high-speed interconnects. The MDA construct the macromodel by cascading multiple CCTL units with corresponding impedance matrix distributions. Although the CCTL unit is a coupled interconnect model under the assumption of homogeneous transmission lines, it has been shown that the macromodel based on the CCTL unit can well predict both the frequency- and time-domain responses of the inhomogeneous coupled interconnects. Two examples have been used to demonstrate the validity of the proposed approach. One is the differential pairs crossing the asymmetrical ground slot. The other is the three coupled microstrip lines. The synthesized macromodel show good accuracy in broadband frequency from dc up to 7 GHz and also excellent time-domain behavior with fast rise time of about 45 ps. The macromodel is suitable for applying in the SPICE simulation of high-speed digital circuits.

References

[1] J. M. Jong, B. Janko, and V. K. Tripathi, "Time-domain characterization and circuit modeling of a multilayer ceramic package," *IEEE Trans. Adv. Packag.*, vol. 19, pp. 48–56, Feb. 1996.

[2] K. D. Marx and R. I. Eastin, "A configuration-oriented spice model for multiconductor transmission lines with homogeneous dielectrics," *IEEE Trans. Microwave Theory Tech.*, vol. 38, pp. 1123–1129, Aug. 1990.

[3] W. T. Beyene and J. Schutt-Aine, "Accurate frequency-domain modeling and efficient circuit simulation of high-speed packaging interconnects," *IEEE Trans. Microwave Theory Tech.*, vol. 45, pp. 1941–1947, Oct. 1997.

[4] T. Mangold and P. Russer, "Full-wave modeling and automatic equivalent-circuit generation of millimeter-wave planar and multilayer structures," *IEEE Trans. Microwave Theory Tech.*, vol. 47, pp. 851–858, June 1999.

[5] S. Myunghee, R. Woonghwan, K. Hyungsoo, K. Jonghoon, and K. Joungho, "An efficient crosstalk parameter extraction method for high-speed interconnection lines," *IEEE Trans. Adv. Packag.*, vol. 23, pp. 148–155, May 2000.

[6] A. Sutono, N. G. Cafaro, J. Laskar, and M. M. Tentzeris, "Experimental modeling, repeatability investigation and optimization of microwave bond wire interconnects," *IEEE Trans. Adv. Packag.*, vol. 24, pp. 595–603, Nov. 2001.

[7] K. Naishadharn, "Experimental equivalent-circuit modeling of SMD inductors for printed circuit applications," *IEEE Trans. Electromagn. Compat.*, vol. 43, pp. 557–565, Nov. 2001.

[8] B. J. Cooke, J. L. Prince, and A. C. Cangellaris, "S-parameter analysis of multiconductor integrated circuit interconnect systems," *IEEE Trans. Computer-Aided Design*, vol. 11, pp. 353–360, Mar. 1992.

[9] B. Young, "Wide-band 2N-port S-parameter extraction from N-port data," *IEEE Trans. Microwave Theory Tech.*, vol. 46, pp. 1324–1327, Sept. 1998.

[10] K. L. Cho, N. Na, and M. Swaminathan, "Characterization of embedded passives using macromodels in LTCC technology," *IEEE Trans. Comp., Packag., Manufact. Technol. B*, vol. 21, pp. 258–268, Aug. 1998.

[11] R. Mittra and U. Pekel, "A new look at the perfectly matched layer (PML) concept for the reflectionless absorption of electromagnetic waves," *IEEE Microwave Guided Wave Lett.*, vol. 5, pp. 84–86, Mar. 1995.

[12] D. M. Sheen, S. M. Ali, M. D. Abouzahra, and J. A. Kong, "Application of the three-dimensional finite-difference time-domain method to the analysis of planar microstrip circuits," *IEEE Trans. Microwave Theory Tech.*, vol. 38, pp. 849–857, July 1990.

[13] S. C. Burkhart and R. B. Wilcox, "Arbitrary pulse shape synthesis via nonuniform transmission lines," *IEEE Trans. Microwave Theory Tech.*, vol. 38, pp. 1514–1518, Oct. 1990.

[14] C. W. Hsue and T. W. Pan, "Reconstruction of nonuniform transmission lines from time-domain reflectometry," *IEEE Trans. Microwave Theory Tech.*, vol. 45, pp. 32–38, Jan. 1997.

[15] C. Schuste and W. Fichtne, "Signal integrity analysis of interconnects using the FDTD method and a layer peeling technique," *IEEE Trans. Electromagn. Compat.*, vol. 42, pp. 229–233, May 2000.

[16] S. Pannala, A. Haridass, and M. Swaminathan, "Parameter extraction and electrical characterization of high density connector using time domain measurements," *IEEE Trans. Adv. Packag.*, vol. 22, pp. 32–39, Feb. 1999.

[17] D. A. Smolyansky and S. D. Corey, "Characterization of differential interconnectsfrom time domain reflectometry measurement," Tech. Rep., TDA Systems Inc., 2004.

[18] L. A. Hayden and V. K. Tripath, "Characterization and modeling of multiple line interconnections from time domain measurements," *IEEE Trans. Microwave Theory Tech.*, vol. 42, pp. 1737–1743, Sept. 1994.

[19] S. D. Corey and A. T. Yang, "Automatic netlist extraction for measurement-based characterization of off-chip interconnect," *IEEE Trans. Microwave Theory Tech.*, vol. 45, pp. 1934–1940, Oct. 1997.

Tzong-Lin Wu (S'93–M'98) was born in Hsinchu, Taiwan, R.O.C., on June 23, 1969. He received the B.S.E.E. and Ph.D. degrees from National Taiwan University, Taipei, Taiwan, R.O.C., in 1991 and 1995, respectively.

From 1995 to 1996, he was a Senior Engineer with Microelectronics Technology, Inc., Hsinchu, Taiwan, R.O.C. (a wireless/Satellite Communication Company dedicated to the development of RF modules). From 1996 to 1998, hewas with the Central Research Institute, Tatung Company, Taipei, Taiwan, where he was involved with the analysis and measurement of EMC/EMI problems of high-speed digital systems. In August 1998, he joined the faculty of the Electrical Engineering Department, National Sun Yat-Sen University (NSYSU), Kaohsiung, Taiwan, where he is currently an Associate Professor. His research interests include design and analysis of fiberoptic components, EMC/SI for high-speed digital systems, and RF circuits design.

Dr. Wu received the Excellent Research Award from NSYSU in 2000 and the Outstanding Young Engineers Award from the Chinese Institute of Electrical Engineers in 2002. He is listed in *Marquis Who's Who in the World* in 2001 and is a member of the Chinese Institute of Electrical Engineers.

Chun-Chih Kuo was born in Taizhong, Taiwan, R.O.C., on August 18, 1977. He received the B.S.E.E. and M.S.E.E. degrees from National Sun Yat-Sen University, Kaohsiung, Taiwan, in 1999 and 2001, respectively, where he is currently pursuing the Ph.D. degree.

His current research interests in the area of numerical electromagnetic field analysis and equivalent model extraction for high-speed digital circuit.

Chen-Chao Wang was born in Miaoli, Taiwan, R.O.C. on February 8, 1973. He received the M.S.E.E. degree in electronic engineering from the National Taiwan University of Science and Technology, Taipei, in June 1998 and is currently pursuing the Ph.D. degree in electrical engineering at National Sun Yat-sen University, Kaohsiung, Taiwan.

From July 1998 to September 2003, he was a Research Assistant at the Industrial Technology Research Institute, Hsinchu, Taiwan. His research interests include signal integrity and power integrity in high-speed digital systems.

Authorized licensed use limited to: Sungmao Wu. Downloaded on May 24,2021 at 05:59:05 UTC from IEEE Xplore. Restrictions apply.

Sung-Moa Wu was born in Kaohsiung, Taiwan, R.O.C., in 1971. He received the Ph.D. degree from the Department of Electrical and Electronic Engineering, National Sun Yat-Sen University, Taipei, Taiwan, in 2001.

During the Ph.D. research he focused on electrical modeling of IC packages. He is currently a Senior Project Engineer with the Electrical Laboratory, Core Capability Center, Advanced Semiconductor Engineering, Inc., Taipei. His research is on high-frequency/high-speed electrical characterization using both simulation and measurement technologies for IC packages

Chih-Pin Hung was born in Taipei, Taiwan, R.O.C., in 1968. He received the Ph.D. degree from the Department of Electrical and Electronic Engineering, University of Paisley, U.K., in 1996.

His research was focused on noise canceling technology of digital signal processing. He is currently Director of the Design Engineering Division, Core Capability Center, Advanced Semiconductor Engineering, Inc., Taipei, Taiwan. His research is in integrated design and electrical characterization of IC packaging.

Authorized licensed use limited to: Sungmao Wu. Downloaded on May 24,2021 at 05:59:05 UTC from IEEE Xplore. Restrictions apply.